Discover Geoscience

Hydrocarbon prospective study using seismic inversion and rock physics in an offshore field, Niger Delta

Ayodele O. Falade[1,2] · John O. Amigun[2] · Olubola Abiola[2]

Abstract

This study integrates seismic inversion and rock physics techniques to evaluate the hydrocarbon potential of an offshore field in the Niger Delta. Five wells revealed three reservoir sands with favourable reservoir properties, including gross thickness (49.2–81.4 m), porosity (0.18–0.2), permeability (565–1481 mD), and water saturation (0.16–0.54). A robust wavelet extraction process was implemented to guide seismic inversion, and a well log-centric approach was employed to validate the resulting acoustic impedance data. Rock physics analysis established correlations between acoustic impedance (Z_p), porosity, fluid content, and lithology, enabling the identification of hydrocarbon-filled sands, brine-saturated sands, and shales. These relationships enabled the discrimination of hydrocarbon-filled sands [5000–8000 (m/s)(g/cc)], from brine-saturated sands [5600–8400 (m/s)(g/cc)], and shales [5000–9000 (m/s)(g/cc)] within the inverted seismic data. The inverted acoustic impedance section showed a general increase with depth, reflecting the typical compaction effects in the Niger Delta. Analysis of the impedance distribution across horizon time slices revealed prospective zones with low impedance values [below 6300 (m/s)(g/cc)], particularly in horizons 1 and 2. These newly identified zones exhibit the strongest potential for hydrocarbon accumulation and warrant further investigation. This study demonstrates the effectiveness of using well log and rock physics constrained seismic inversion for hydrocarbon exploration in an offshore field in the Niger Delta.

Keywords Reservoir properties · Seismic inversion · Acoustic impedance · Rock physics · Hydrocarbon prospects

1 Introduction

The demand for oil and gas continues to rise annually, necessitating the maximization of hydrocarbon production from all potential sources due to the depletion of proven reserves. The Organization of the Petroleum Exporting Countries (OPEC) forecasts a significant rise in global energy demand by 2035, with fossil fuels, remaining the primary source [1]. Consequently, the petroleum industry is constantly seeking innovative approaches to optimize hydrocarbon production and improve reservoir characterization [1–4]. A key challenge in reservoir exploration lies in accurately assessing reservoir heterogeneity which refers to the variation in reservoir properties across a reservoir. Conventional exploration methods often lack the resolution necessary to fully capture this complexity. Therefore, the industry demands models with improved resolution capable of effectively measuring and predicting these crucial reservoir properties [5, 6]. 3D

✉ Ayodele O. Falade, ayofalade@achievers.edu.ng; ayouseh2003@gmail.com; John O. Amigun, johnamigun@gmail.com; Olubola Abiola, oabiola@futa.edu.ng | ¹Department of Geological Sciences, College of Natural and Applied Sciences, Achievers University Owo, PMB 1030, Owo, Ondo State, Nigeria. ²Department of Applied Geophysics, School of Earth and Mineral Science, Federal University of Technology Akure, PMB 704, Akure, Ondo State, Nigeria.

reservoir modeling has proven effective in delineating the geometry of sand bodies, offering a solution to the challenge of subsurface heterogeneity [7, 8]. Additionally, it has been successfully applied in the Niger Delta basin to assess and detect hydrocarbon prospects [7]. Furthermore, geostatistical techniques can be integrated to populate and distribute various reservoir properties across an oilfield, aiding in the identification of prospective zones within the Niger Delta [7, 8].

Seismic amplitude inversion, offers a detailed and reliable view of the subsurface, playing a crucial role in estimating critical reservoir properties like net pay and porosity [9–12]. This technique is widely used in the petroleum industry due to its ability to enhance data resolution and reliability. Information derived from the elastic properties of rocks is essential for characterizing reservoirs and relating them to quantifiable properties. This approach has the potential to discriminate between reservoirs based on their fluid content and composition, with prospective hydrocarbon-saturated areas typically exhibiting low acoustic impedance, lambda-rho, and density [9, 13, 14]. Model-based inversion techniques have proven valuable for prospect mapping and reservoir property estimation [9, 15–19]. However, the reliability of seismic inversion processes is crucial and should be carefully assessed before implementation. Key factors influencing the accuracy of seismic inversion include the choice of wavelet and the correlation between seismic impedance and well log impedance [20, 21]. Notably, researchers often overlook the importance of comparing seismic impedance with impedance from multiple well logs within a field to ensure consistency and accuracy before conducting seismic inversion [22–25]. By performing thorough comparisons using multiple wells, the inversion process can be significantly improved, yielding more reliable petrophysical properties for robust reservoir characterization and development.

Rock physics is key in hydrocarbon prospecting as it offers the basis for understanding the fundamental relationships between rock elastic parameters and reservoir properties. These relationships provide valuable insights into the lithology, porosity, and pore fluid content of reservoirs by analyzing their seismic response [26]. Rock physics workflows typically involve correlating reservoir properties with elastic parameters using characterization models to differentiate reservoirs based on fluid content and lithology [27, 28]. Elastic parameters like impedance, seismic velocity, velocity ratio, Poisson's ratio, mu-rho, and lambda-rho play crucial roles in reservoir studies, with their sensitivity to reservoir properties varying based on the rock type and seismic data quality. Researchers have successfully utilized rock physics models for sensitivity analysis and quantitative seismic inversion interpretation [29–31]. By integrating seismic inversion data with rock physics models, it becomes feasible to predict lithology and fluid content distribution within a reservoir, enhancing the effectiveness of reservoir characterization and exploration efforts [32]. This approach allows for a comprehensive understanding of reservoir properties and facilitates the identification of favourable zones for oil extraction within the studied area.

The prediction and detection of the efficiency of hydrocarbon reservoirs has been greatly increased through seismic inversion and other analyses involving rock physics [33, 34]. This is based on proven relationships between reservoir properties and several elastic parameters at well locations using rock physics principles. This study presents an approach that integrates well log analysis and rock physics constrained seismic inversion for hydrocarbon prospectivity study in an offshore field located in the Niger Delta Basin as most work done using seismic inversion methods have been in the onshore fields. A comprehensive understanding of the subsurface reservoir and its potential for hydrocarbon production will be achieved through this study.

2 Location and geology of study area

This study area is 'OS' field which is located in the near offshore area of the Niger Delta positioned on the Gulf of Guinea basin (Fig. 1). The Niger Delta forms one of the largest hydrocarbon provinces in the world along the West Coast of Central Africa. It covers an area that falls within longitude 5° E–7° 36′ E and latitudes 4° 12′ N–6° 36′ N [35].

The Niger Delta basin is composed of a clastic sequence formed during regression in the Tertiary age [36]. Within the Niger Delta petroleum province, three major stratigraphic units have been identified: Benin, Agbada and Akata Formations [37]. These formations were created through the deposition in the Niger Delta during the Tertiary Epoch. These formations delineate prograding depositional facies established on lithology (i.e. the ratio of sand to shale). The Akata Formation which is found at the base of the delta originates from marine conditions, encompassing a substantial quantity of shale sequences (having source rock potential), turbidite sand (could act as reservoirs in deep water environment), and small amounts of other fine grained sediments (silt and clay). During lowstands, the Akata Formation amassed organic matter and clays of terrestrial origin in deep-water regions marked by low-energy conditions and an absence of oxygen [38].

The Agbada Formation, constituting the primary hydrocarbon-bearing unit, initiated deposition throughout the Eocene epoch and extends into Recent. It comprises paralic siliciclastics with a thickness of over 3700 m, representing
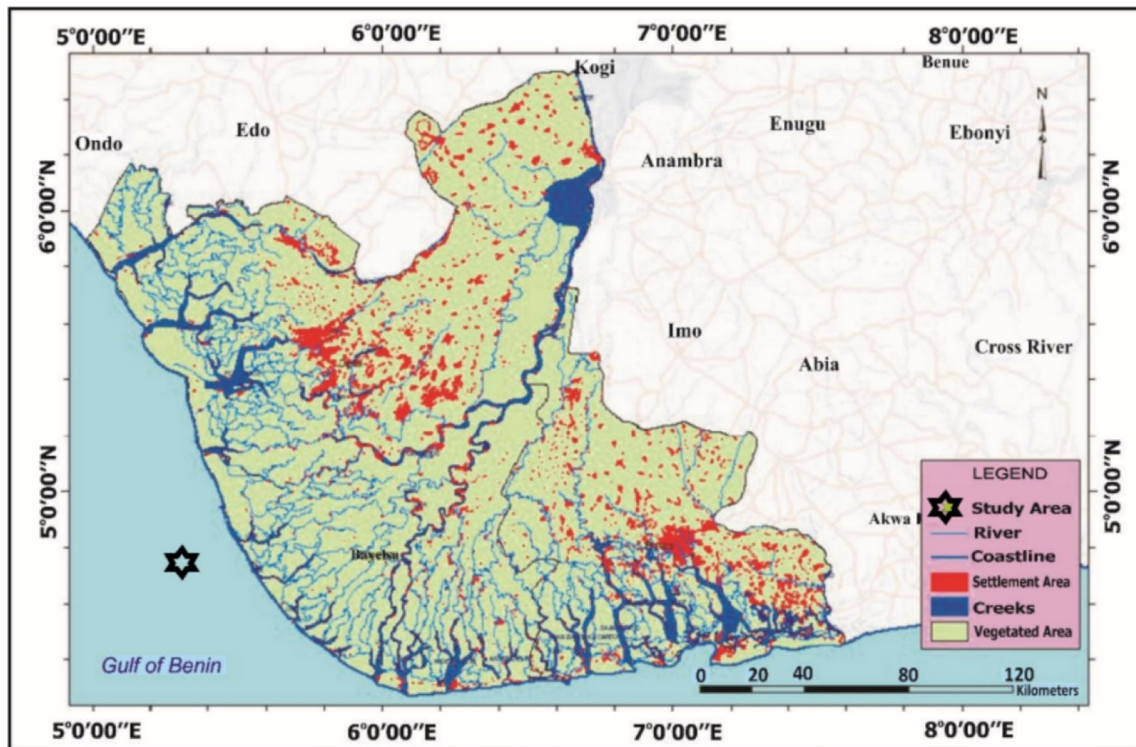
Fig. 1 Niger Delta map showing the study area

the real deltaic segment of the sequence (Fig. 2). Identical proportions of shale and sandstone beds is witnessed at the lower portion of this Formation, while the upper section is primarily composed of sand interbedded with minor shale layers. The Miocene and Pliocene Agbada Formation has been the subject of extensive research on its

Fig. 2 The stratigraphy of Niger Delta from late cretaceous to quaternary [42, 43]

Extent of erosional truncation
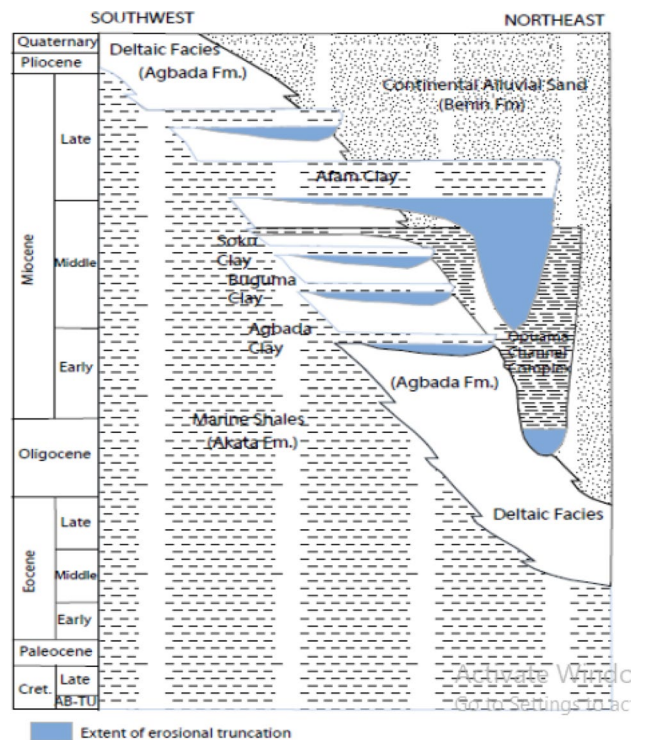
sequence stratigraphy and sedimentary facies, revealing a complex depositional system characterized by delta front, gravity flow channel, and turbidite fan deposits [39, 40]. These facies are critical for understanding the formation's hydrocarbon potential and guiding exploration efforts.

Above the Agbada Formation lies the Benin Formation, composed of deposits from the continental environment spanning from the Eocene epoch to Recent. Its deposits comprise alluvial and upper coastal plain sands, reaching thicknesses of up to 2000 m [41]. This stratigraphic overview provides a foundation for understanding the geological evolution and petroleum potential of the Niger Delta Basin. The geological significance of these formations contributes to the region's proficiency in hydrocarbon production, solidifying its position as a key sedimentary basin in Nigeria (Fig. 2).

3 Research methodology

The data used in this research was obtained from the 'OS' field, situated in the offshore region of the Niger Delta basin in Southern Nigeria. A suite of well logs [Gamma-Ray (GR), resistivity, sonic and density logs] and check shot data for five wells (OS-1, -2, -3, -4 and -5) and post-stack seismic data from the 'OS' offshore field, Niger Delta were used for this study (Fig. 3). The research methodology includes synthetic seismogram generation, well to seismic tie, wavelet extraction, impedance correlation, rock physics and seismic inversion. This study was carried out using Techlog and Hampson Russel software and the workflow is shown in Fig. 4.
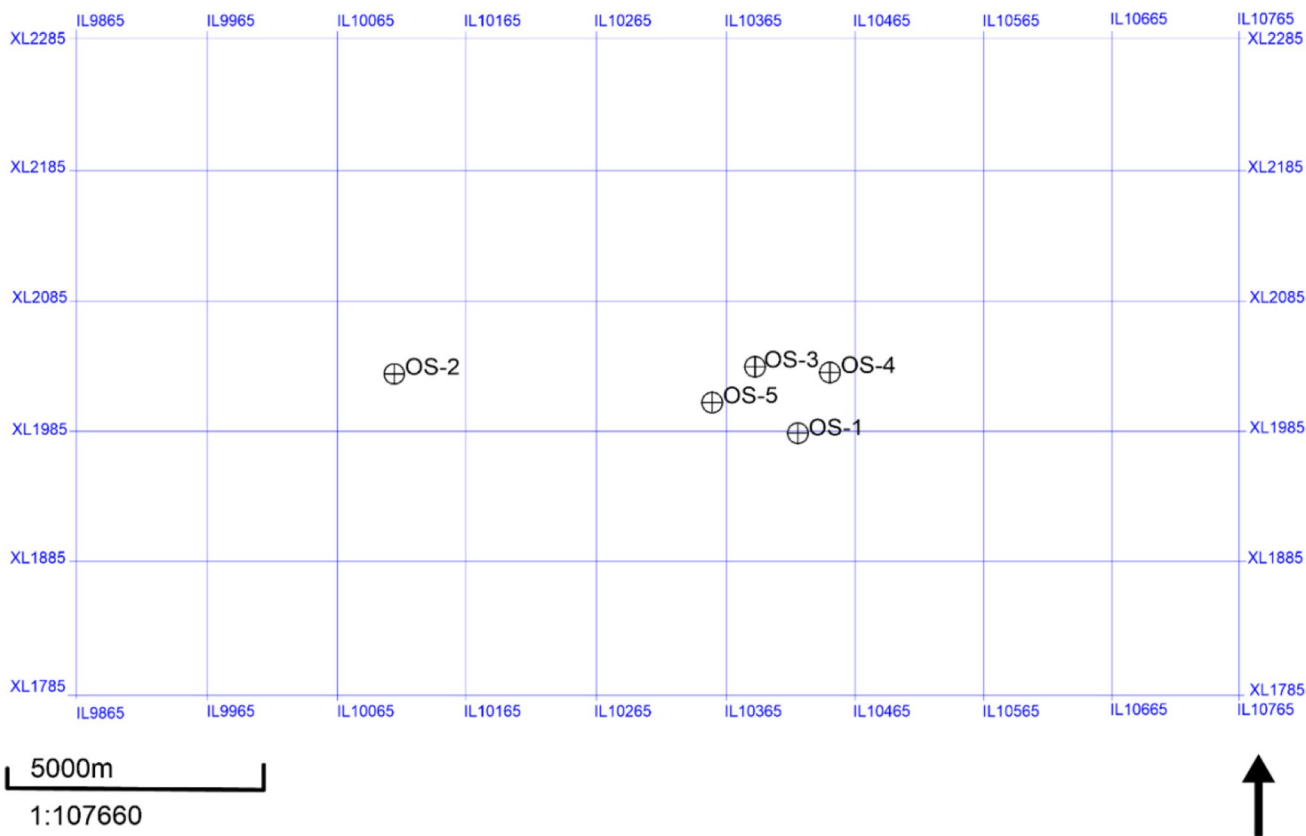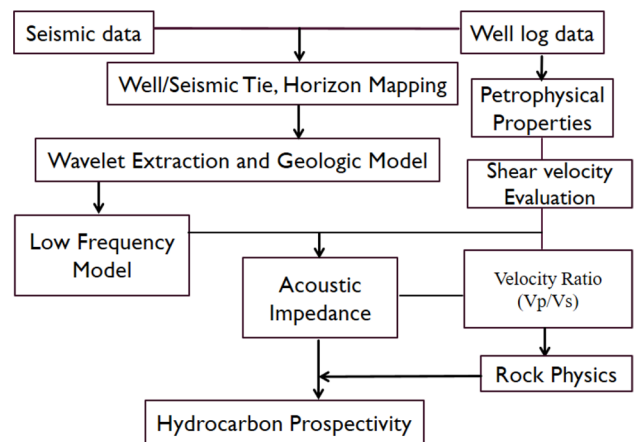

**Fig. 3** Base map of the 'OS' field showing the well locations with the inlines and xlines

Fig. 4 Generalized flow chart
for seismic inversion

3.1 Well log analysis

Intervals corresponding to the reservoirs of interest were delineated from each well log and the wells were correlated using the Gamma-Ray log and resistivity log (Fig. 5). The following petrophysical properties were determined from the well logs after the delineation of reservoirs and correlation across the wells:

i. Volume of shale (V_{sh}): $V_{sh} = 0.083 * \left[2^{(3.7*IGR)} - 1\right]$,   (1)
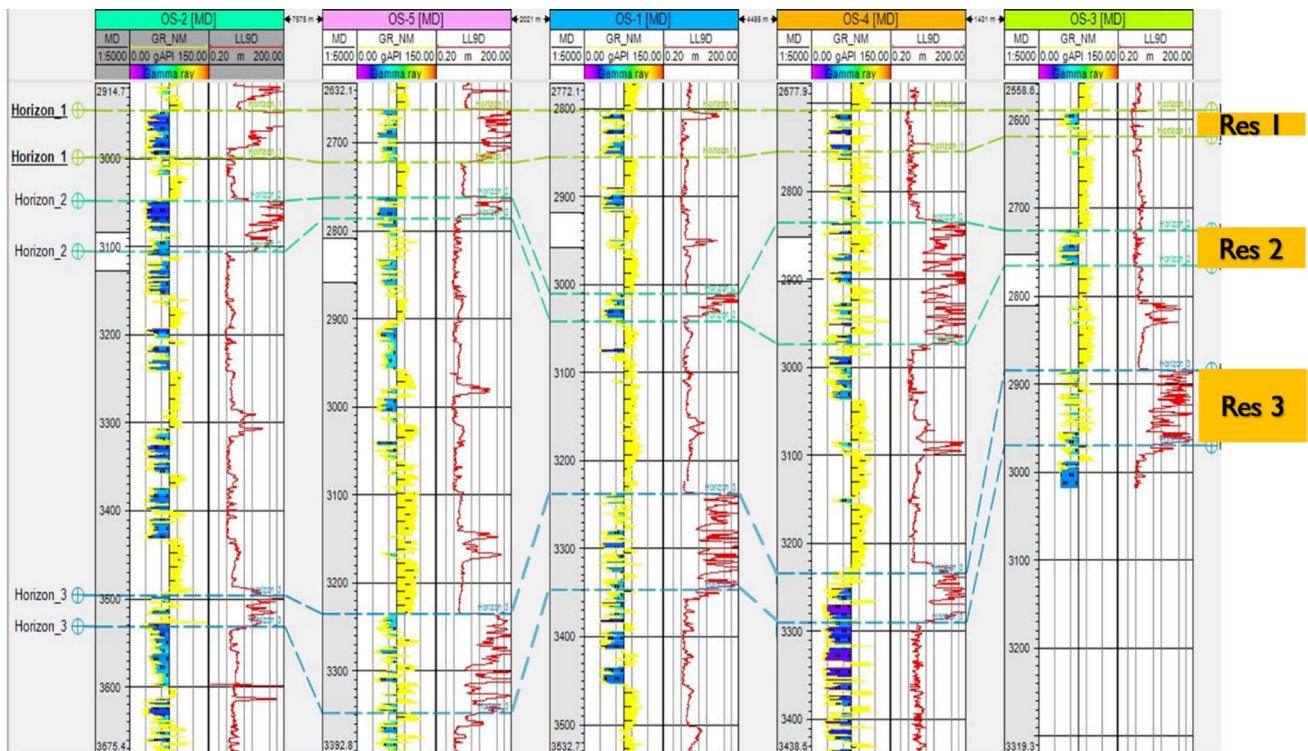
Fig. 5 Well log correlation panel for visual comparison of log responses showcasing the lithological and petrophysical similarities across the available five wells

$$\text{Where IGR} = \frac{GR_{log} - GR_{min}}{GR_{max} - GR_{min}}. \tag{2}$$

where Vsh is Volume of shale [44], IGR is Gamma-Ray index, GR_{log} is Gamma-Ray reading from log, GR_{min} is the Gamma-Ray reading from the cleaniest sandstone and GR_{max} is the Gamma-Ray reading from the most shaliest part of the reservoir.

$$\text{ii.} \quad \text{Net to Gross} = \frac{\text{Net Pay}}{\text{Gross Thickness}}, \tag{3}$$

where net pay is the portion of the delineated reservoirs with presence of hydrocarbon [45].

$$\text{iii.} \quad \text{Porosity}: \phi = \frac{\rho_{ma} - \rho_b}{\rho_{ma} - \rho_f}, \tag{4}$$

where ρma is matrix density, ρb is the density from the well log and ρfl is the fluid density [45].

$$\text{iv.} \quad \text{Water Saturation}: S_w^n = \frac{a \times R_w}{\phi^n R_t}, \tag{5}$$

where Rw is water resistivity, Rt is true resistivity, n is saturation exponent and a is cementation constant.
v. Permeability (k) was estimated using the empirical formula according to Timur [46],

$$k^{1/2} = \frac{250\phi^2}{Swirr}, \tag{6}$$

where Swirr is irreducible water saturation.

3.2 Seismic to well tie

Tying seismic data to the well log forms the basis for the process of any form of seismic interpretation in which the seismic data is properly converted from the time domain to the depth domain. A seismic-to-well tie was established using check shot data, which revealed the relationship between depth and time for the formation (Fig. 6). This tie enabled the conversion of depth values to seismic times, allowing for the accurate mapping of the top of the delineated reservoirs. Well OS-5 was successfully tied to the seismic volume, and the corresponding horizons were mapped (Fig. 7).

3.3 Estimation of inversion parameters

Following the initial petrophysical analysis, synthetic seismogram generation, and seismic-to-well tie, a crucial step is to generate acoustic impedance from well logs and cross-plot it with rock properties derived from well logs, prior

Fig. 6 Time to depth graph showing the relationship between seismic travel times and corresponding depths thereby allowing the integration of seismic and well log data
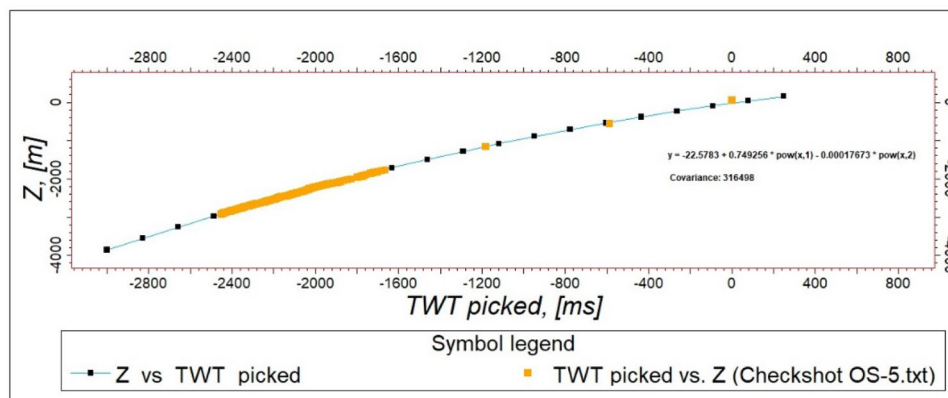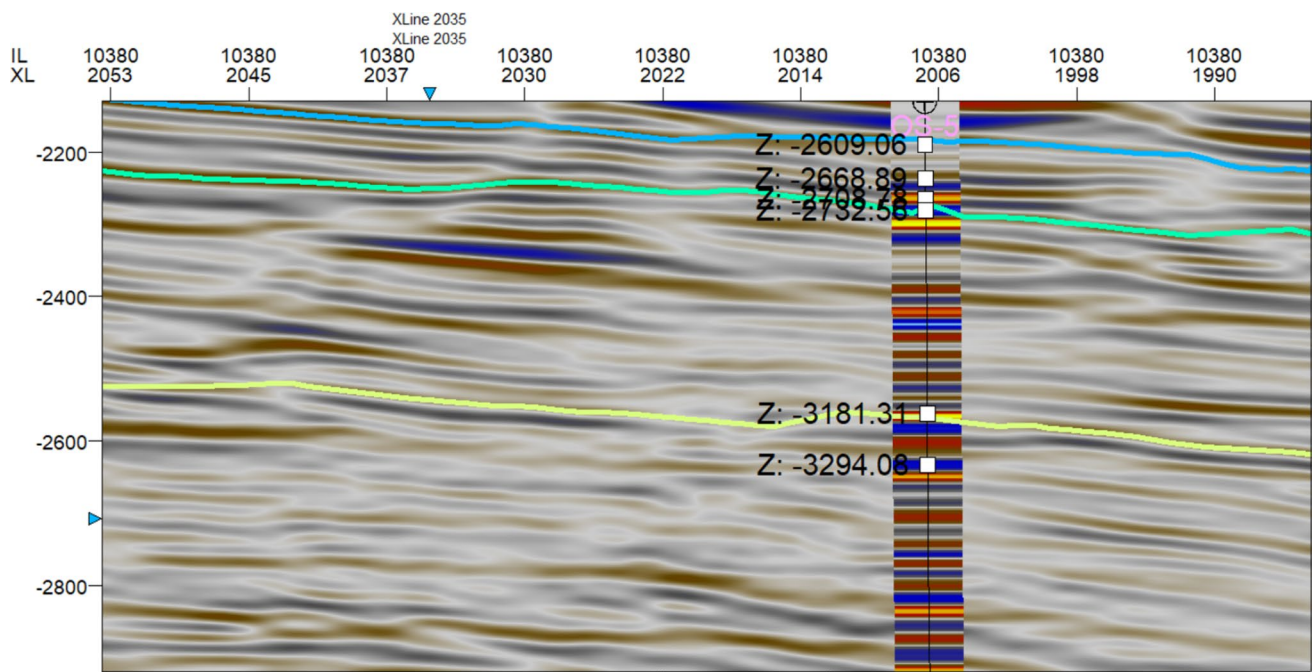
Fig. 7 Seismic to well tie using well OS-5, with the depth of the top and base of the reservoirs displayed

to conducting seismic inversion. The equations applied in the estimation of inversion parameters (Vp, Vs, Zp and Zs) from well logs are shown in Eqs. (7–10) [47–49].

$$Vp = (1000000/DTc) \times 0.3281, \tag{7}$$

$$Zp = V_p \times \rho_b. \tag{8}$$

The secondary velocity (Vs) was estimated according to the relationship by Greenberg and Castagna [50] for siliciclastic rocks.

$$Vs = 0.8042Vp - 0.8559, \tag{9}$$

$$Zs = V_s \times \rho_b, \tag{10}$$

where Vp is primary velocity, Vs is secondary velocity, Zp is P-impedance, Zs is S-impedance, DTc is compressional sonic log, ρ_b is density from bulk density log.

3.4 Rock physics

A cross plot of Zp and Zs (Fig. 8) was used to validate the applicability of the empirical formula by Greenberg and Castagna [50] in Eq. (9), revealing a direct relationship that confirms the usability of the equation for estimating Zs. The estimated inversion parameters were then utilized to establish their relationship with other reservoir properties through rock physics analysis in a 3D space. This rock physics analysis involved generating two key cross-plots. The first cross-plot displays acoustic impedance versus porosity, coloured by Gamma-Ray values for lithological identification and water saturation for fluid content. The second cross-plot shows Vp/Vs versus P-impedance (Zp), coloured by water saturation. These cross-plots enabled the quantitative interpretation of the inversion method, allowing for the extraction of impedance values corresponding to hydrocarbon-bearing sands. This integrated analysis facilitated the identification of reservoir properties and fluid content, enhancing the understanding of the subsurface geology.
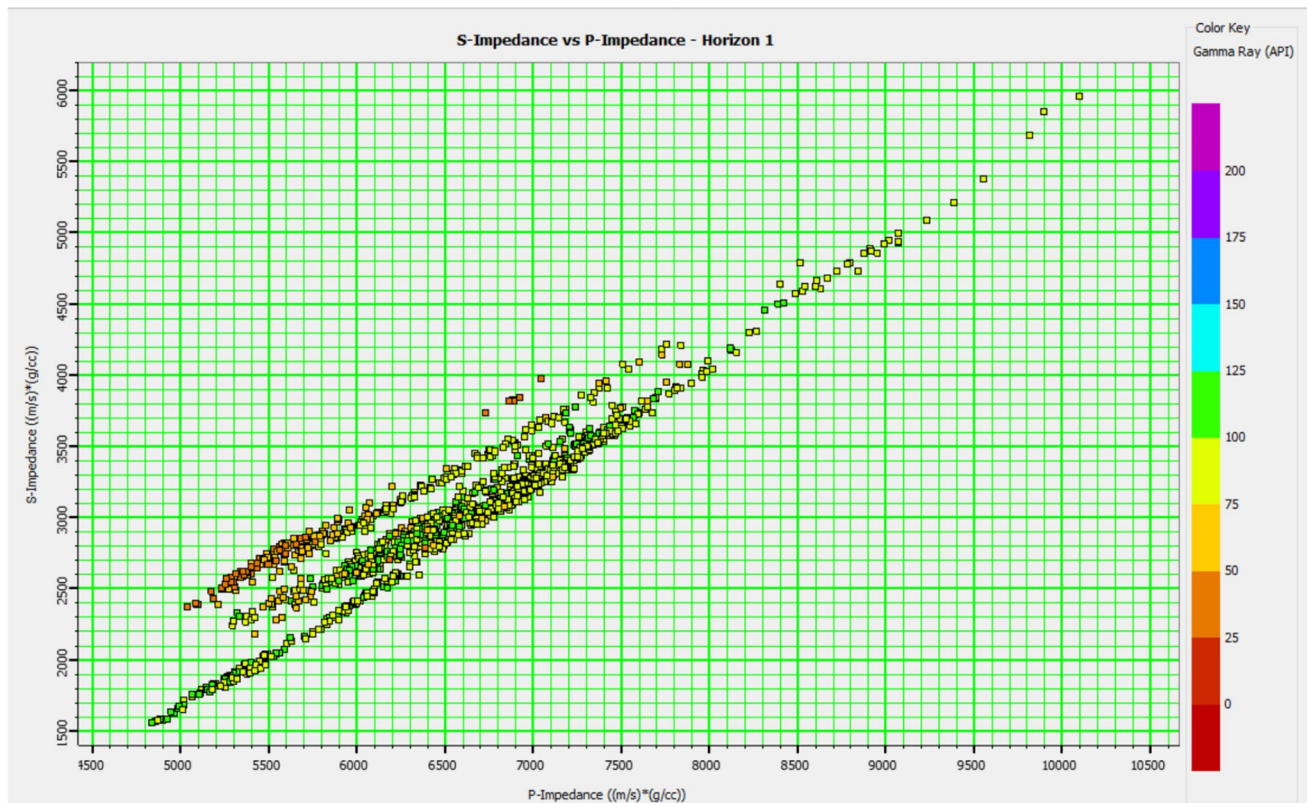
Fig. 8 Cross plot showing the relationship of the estimated Zp and Zs as a quality control for the estimation of Vs from well logs

3.5 Seismic inversion

Wavelet extraction was performed to deconvolve the seismic data, yielding the subsurface's reflectivity series via the seismic inversion convolution model (Eq. 11). This crucial step enabled the retrieval of the underlying reflectivity series from the seismic data, providing valuable insights into the subsurface's geological structure.

$$S(t) = W(t) * R + N. \tag{11}$$

S(t) is the recorded seismic trace, W(t) is the seismic wavelet, R is the Earth's reflectivity series, and N is the added noise [47, 48, 51].

This study utilized extracted statistical wavelet, W(t), representing the source and recording system's filtering effect, to correlate both reflectivity (extracted and inverted) derived at all wells. A cross-correlation analysis was employed for wavelet extraction from seismic data by assessing the similarity between the data and potential wavelets. This involved calculating the cross-correlation coefficient between the seismic trace and each possible wavelet. The extraction process utilized a zero-degree phase rotation, with a lag time of 100 ms and a variable window length range per well, optimized in the time domain to achieve the maximum cross-correlation coefficient. This process was repeated for all wells, and the wavelet with the highest coefficient was selected for each well. Maintaining a minimum-phase wavelet is crucial for reliable seismic interpretation and inversion, so, a low-phase wavelet (29°) was used in this study. This is because significant phase shifts in the input wavelet can significantly impact the inversion results, leading to higher errors in the final impedance data [52].

Quality control was conducted after seismic to well tie and wavelet extraction was carried out to check the consistency of the seismic impedance and the well log impedance from well location path. An initial P-impedance model was created using well logs and mapped horizons to enable model-based seismic inversion to be applied (Fig. 9a). This crucial step enabled the inversion of seismic data into a 3D volume of impedance values, providing a more accurate and geologically consistent representation of the subsurface properties (Fig. 9b).
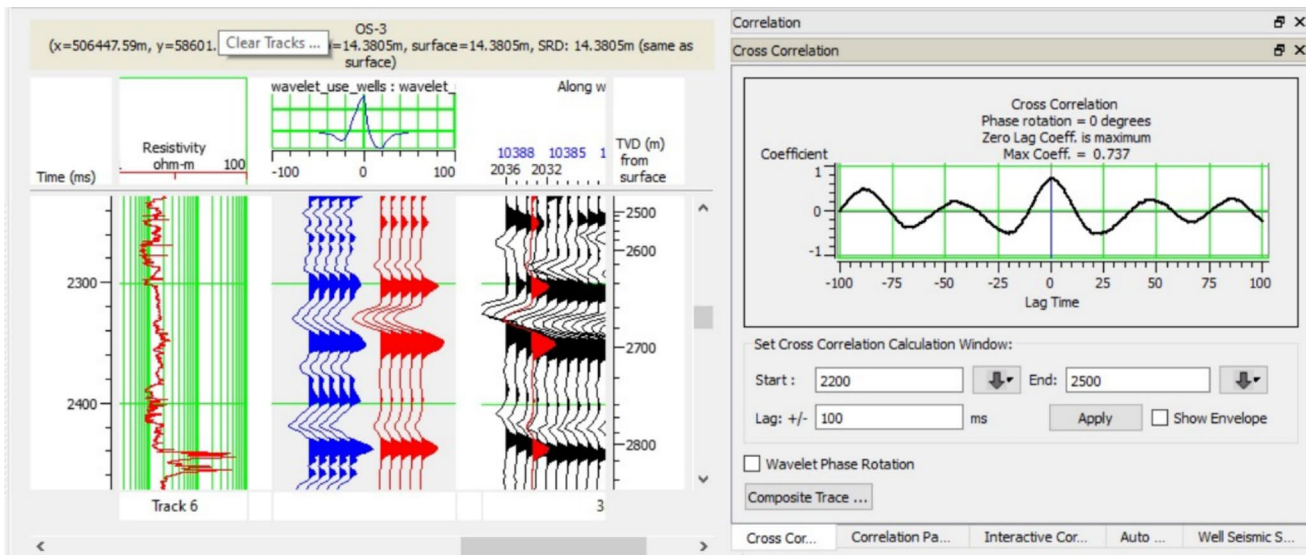
(a)
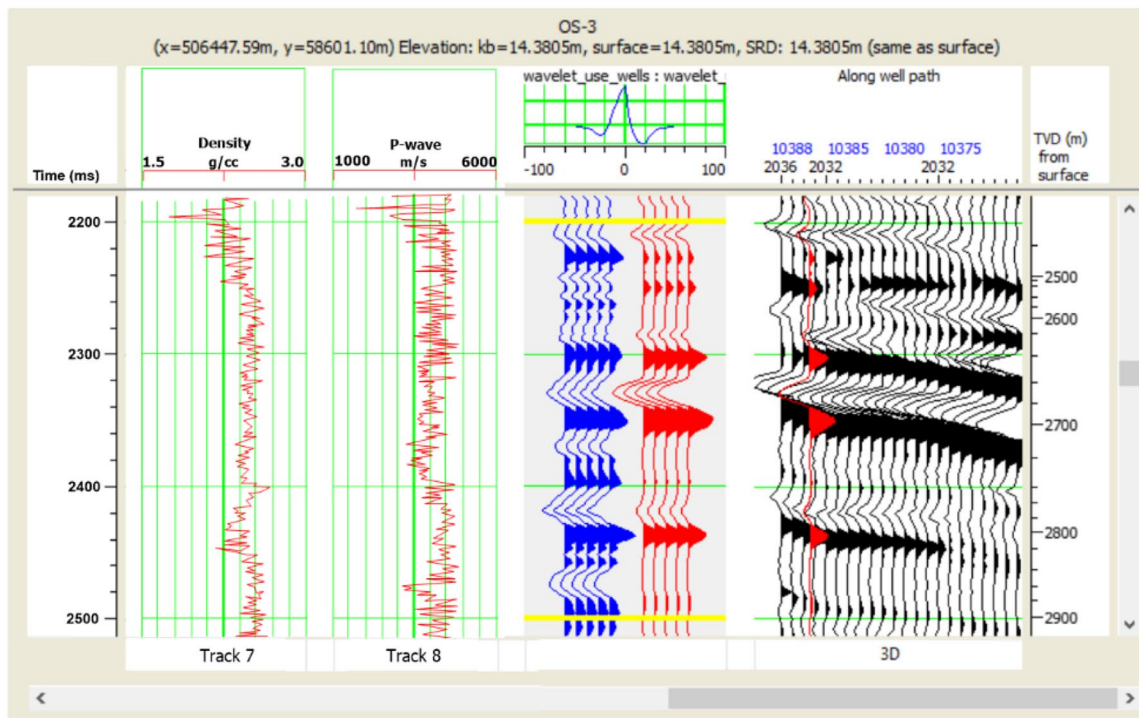
(b)

Fig. 9 **a** Seismogram analysis and estimation of wavelet using selected seismic traces for OS-3 well showing the extraction and valuable information from seismic data **b** synthetic seismogram of OS-3

4 Results and discussion

4.1 Well log analysis

Three reservoir sands were delineated from the five available wells in the study area. The average estimated reservoir

Table 1 Average estimated reservoir parameters for delineated reservoirs

Reservoir	Gross thickness (m)	Net pay (m)	NTG	Vsh	Porosity	Permeability (mD)	Sw	Sh
1	49.2	26.4	0.54	0.12	0.2	1481	0.54	0.46
2	58.8	47.2	0.80	0.15	0.19	1404	0.16	0.84
3	81.4	73.8	0.91	0.31	0.18	565	0.17	0.83
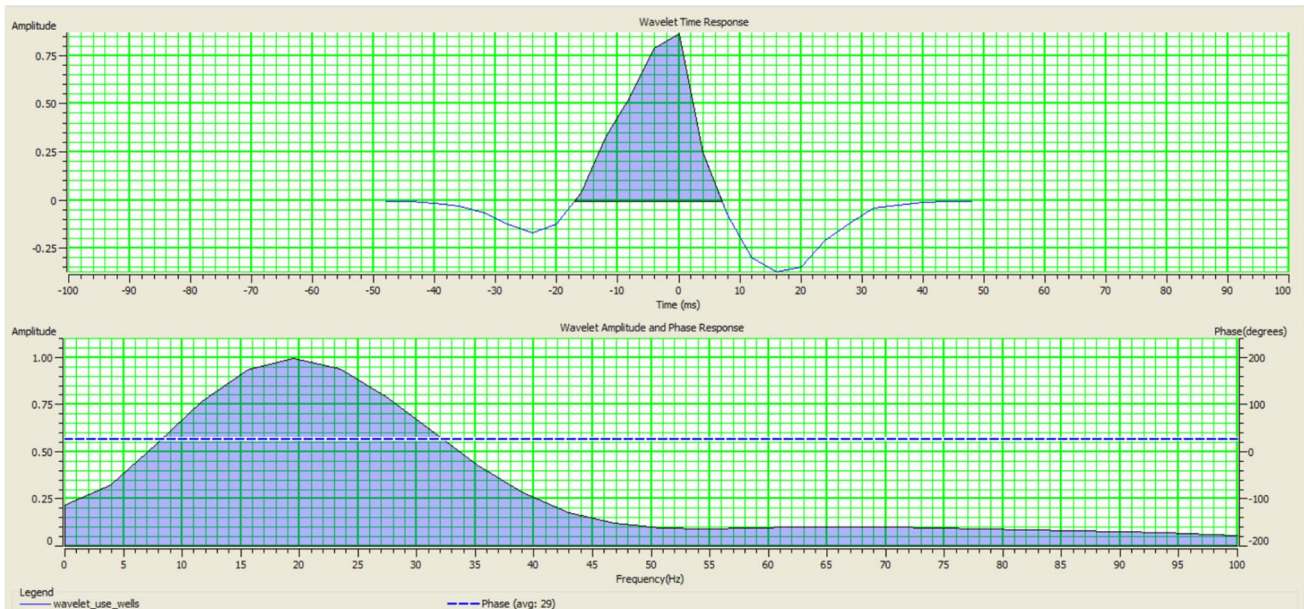
Fig. 10 Wavelet extracted in the time domain (top) and frequency domain (down) representing the seismic character of the source

properties of all reservoirs across all wells are summarized in Table 1. The gross thickness (GT) of the reservoirs ranges from 49.2 to 81.4 m, while the net pay thickness varies from 26.4 to 73.8 m. The net pay to gross ratio (NTG) spans from 0.54 to 0.91, indicating the proportion of the reservoir that contributes to hydrocarbon production. The volume of shale (Vsh) content ranges from 0.12 to 0.31, reflecting the extent of non-reservoir material within the sands. Porosity values, crucial for assessing the storage capacity of the reservoirs, range from 0.18 to 0.20. Permeability, which indicates the ability of fluids to flow through the reservoir rocks, varies significantly between 565 to 1481 mD. Water saturation levels, an indicator of the amount of water present in the pore space, range from 0.16 to 0.54. The well log analysis revealed that all delineated reservoirs generally exhibit good reservoir properties, indicating their viability for hydrocarbon production. Among the reservoirs, Reservoir 1 was identified as having the least favorable properties. Despite this, the overall quality of the reservoirs suggests a promising hydrocarbon potential within the study area.

4.2 Wavelet extraction

A statistical technique called cross-correlation analysis was applied to extract the seismic wavelet from the seismic data volume, utilizing the available wells in the study area. This extracted wavelet serves as the fundamental building block of the seismic response and is crucial for accurate seismic inversion. Cross-correlation analysis revealed that the statistical wavelet with OS-3 exhibited the highest correlation coefficient (0.737) with the seismic data within a time window of 2200–2500 ms (Fig. 9a, b). This window represents the optimal wavelet that best characterizes the seismic data, essential for accurate seismic inversion. Following this identification, the wavelet was further characterized by a 29° phase shift and a dominant frequency range of 0–50 Hz (Fig. 10). The extracted wavelet with these properties was then employed for acoustic impedance estimation from the seismic data.

4.3 Quality control

A prior analysis was conducted to establish a robust correlation between the impedance values derived from seismic data and well logs by correlating impedance from seismic and well logs before applying seismic inversion to the seismic volume. Figure 11a–e illustrates this correlation at all well location, covering different time interval per well. A strong correlation is evident, with low error values ranging from 385.225 to 520.235 across all wells, indicating excellent consistency between the seismic response and well log data. Moreover, the relative error values fall within an acceptable range, further validating the accuracy of the inversion process for the post-stack seismic data [53–55]. This ensures that the derived impedance profiles accurately represent the subsurface geology, providing a reliable basis for reservoir characterization and decision-making.

Furthermore, a synthetic seismic trace generated from the inverted impedance (shown in red in Fig. 11) exhibits an exceptionally high correlation coefficient (0.992808) with the actual seismic trace (black) around the potential reservoir intervals in well OS-3. This strong correlation provides added confidence in the reliability of the inverted acoustic impedance data used for subsequent hydrocarbon prospectivity analysis. Having established the robustness of the correlation and the accuracy of the inversion process through these quality control measures, we proceeded with full seismic inversion to generate the final acoustic impedance models for the study area.

4.4 Rock physics

The analysis of rock properties in 3D space revealed significant correlations with reservoir characteristics, particularly fluid content and lithology. These connections are crucial for the quantitative interpretation of seismic inversion results for reservoir characterization in the 'OS' offshore field. A cross-plot of Zp versus porosity, colour-coded with Gamma-Ray (GR) for lithology discrimination (Fig. 12a), exhibited a linear trend. Sand bodies identified through this cross-plot are characterized by Zp values ranging from 5000 to 8000 (m/s)(g/cc), porosity values greater than 0.13, and Gamma-Ray readings below 75 API. In contrast, shales exhibit Zp values from 5000 to 9000 (m/s)(g/cc), porosity values less than 0.13, and Gamma-Ray readings over 75 API. When colour-coded with water saturation, this cross-plot enabled the differentiation of reservoirs into hydrocarbon-filled sands, brine-saturated sands, and shales (Fig. 12b). Hydrocarbon-bearing sands are delineated by Zp values ranging from 5000 to 7800 (m/s)(g/cc) and lower water saturation values. Brine-filled sands show Zp values between 7400 and 8400 (m/s)(g/cc) and higher water saturation, while shales have Zp values from 5000 to 8800 (m/s)(g/cc) across varying water saturation levels.

Similarly, a cross-plot of the velocity ratio (Vp/Vs) and P-impedance (Zp), colour-coded with Gamma ray and water saturation, were used to distinguish lithology and fluid content respectively (Fig. 13a, b). Hydrocarbon sands are characterized by P-impedance values ranging from 5000 to 7000 (m/s)(g/cc) and a velocity ratio between 1.9 and 2.3, Brine filled sands has a P-impedance value range of 5600 to 7000 (m/s)(g/cc) while the P-impedance (Zp) of shale is between 5000 and 7500 (m/s)(g/cc) and a velocity ratio range of 2.0–3.1. Based on the analysis from the cross-plots, the P-impedance range for hydrocarbon-bearing sands is 5000 to 7800 (m/s)(g/cc), brine-filled sands is 5600 to 7000 (m/s)(g/cc), and shale is 5000 to 9000 (m/s)(g/cc). These findings are consistent with the unconsolidated nature of Niger Delta reservoirs, as noted in previous studies [53, 56, 57].

4.5 Model-based seismic inversion

Figure 14 presents the inverted acoustic impedance section for the 'OS' field, along with the mapped horizons. The results display a general increase in impedance with depth, consistent with the typical compaction effects observed in Niger Delta geology. The inverted impedance values are categorized into distinct classes, ranging from very low [3601–4563 (m/s)(g/cc)] to extremely high (8650–9372 (m/s)(g/cc)), as shown in Table 2. These impedance categories are visually represented by a colour bar in Fig. 15, where purple indicates extremely high impedance and green indicates very low impedance. Rock physics analysis suggests that sand zones correspond to impedance values between 5000 and 8000 (m/s)(g/cc), water-bearing sands exhibit impedance values between 6800 and 8000 (m/s)(g/cc), and shales have an impedance range of 5000–9000 (m/s)(g/cc). This variation is primarily driven by density differences, with shales having higher densities and consequently higher impedance values compared to sand
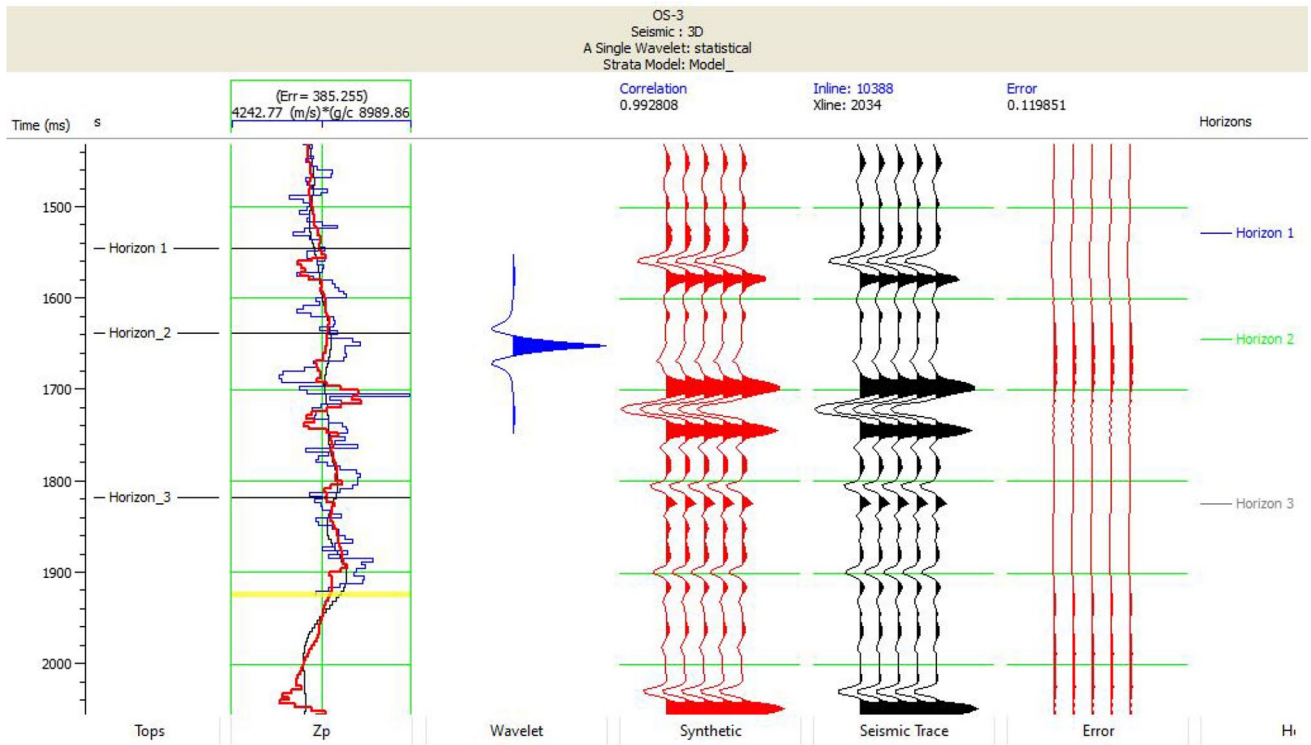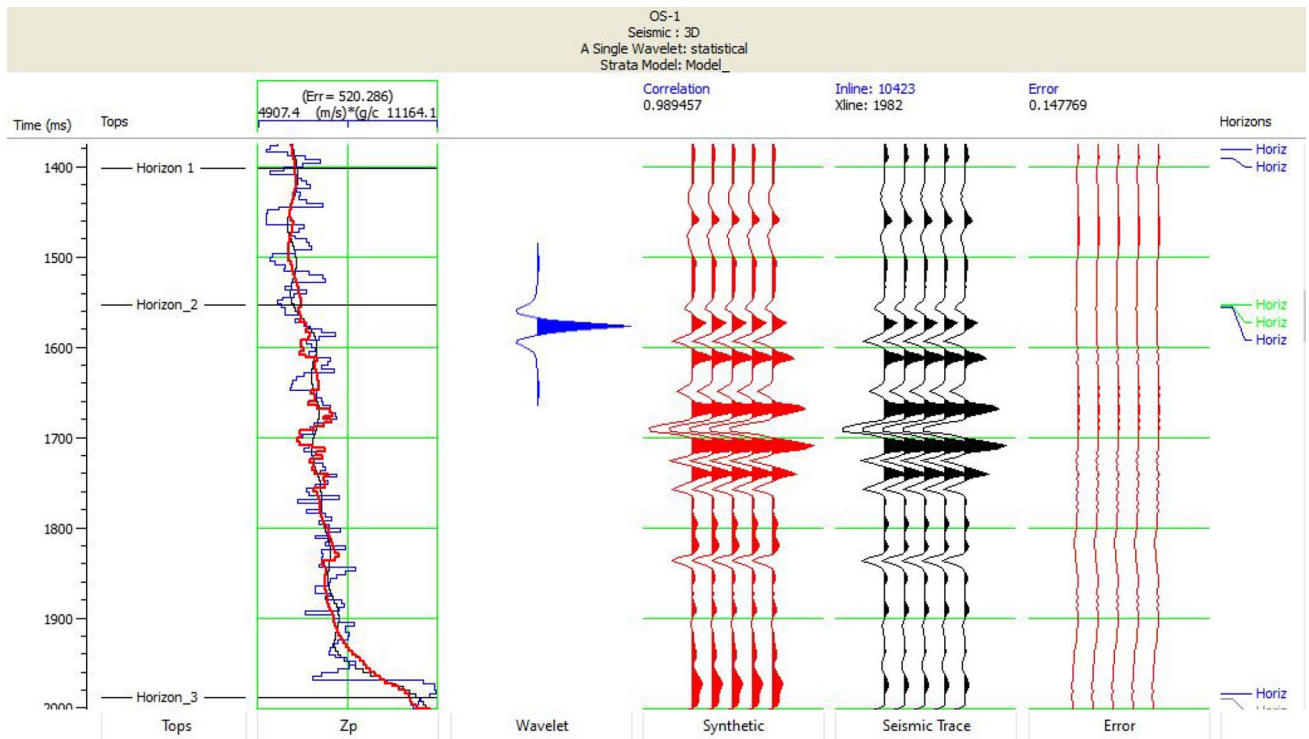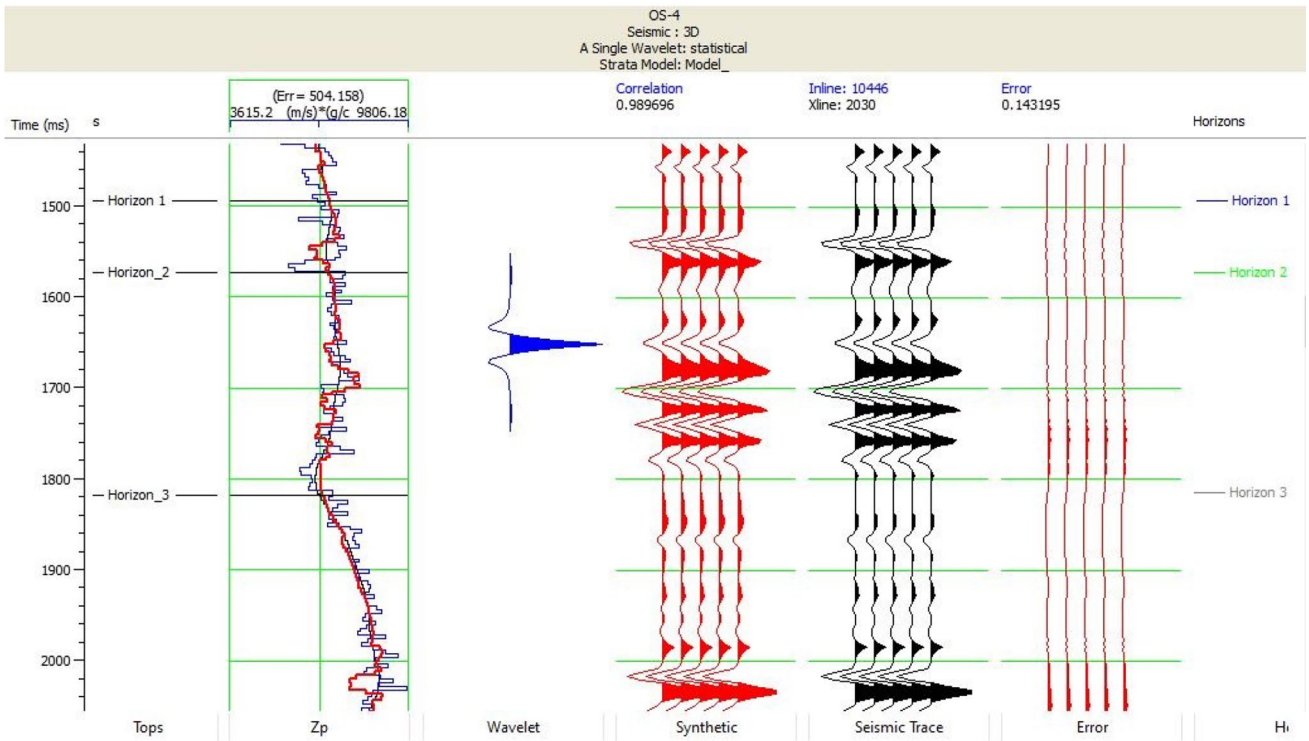
(a)
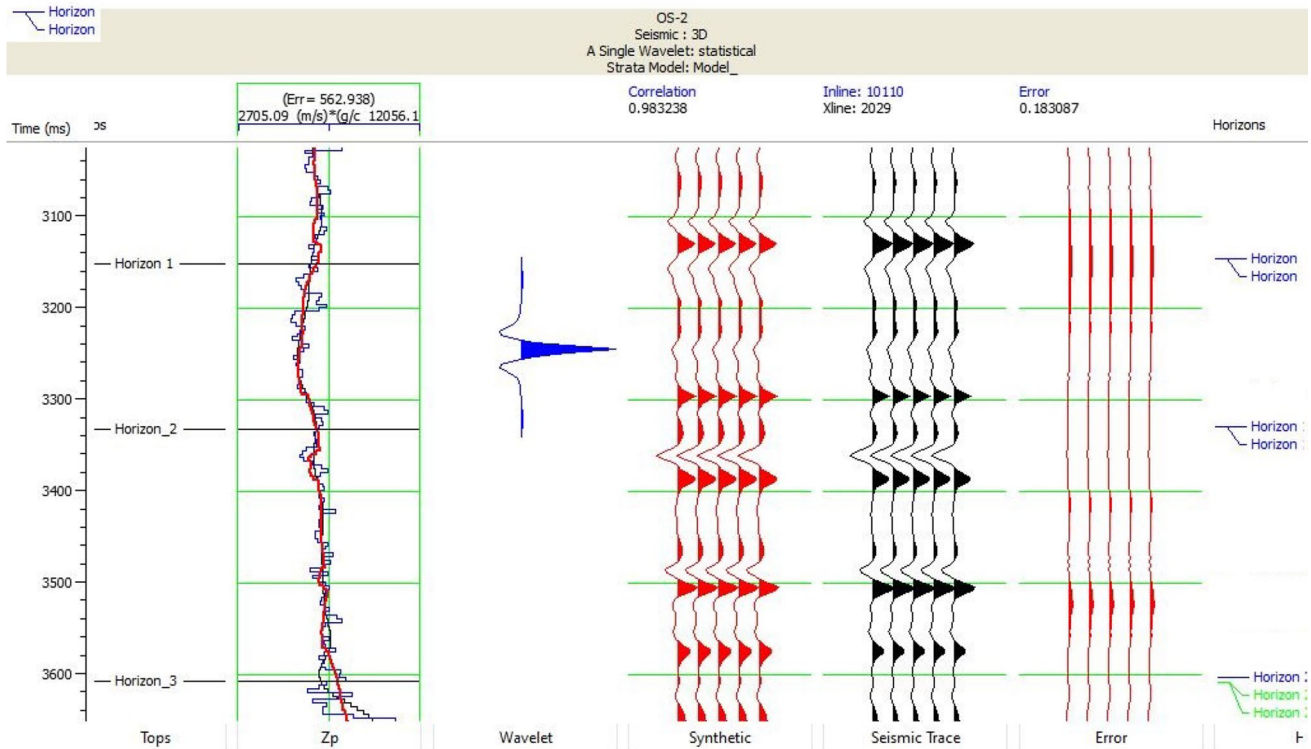
(b)

Fig. 11 Seismic inversion quality control analysis comparing the impedance and seismic traces derived from seismic and well log data for **a** OS-3 **b** OS-2 **c** OS-1 **d** OS-4 **e** OS-5
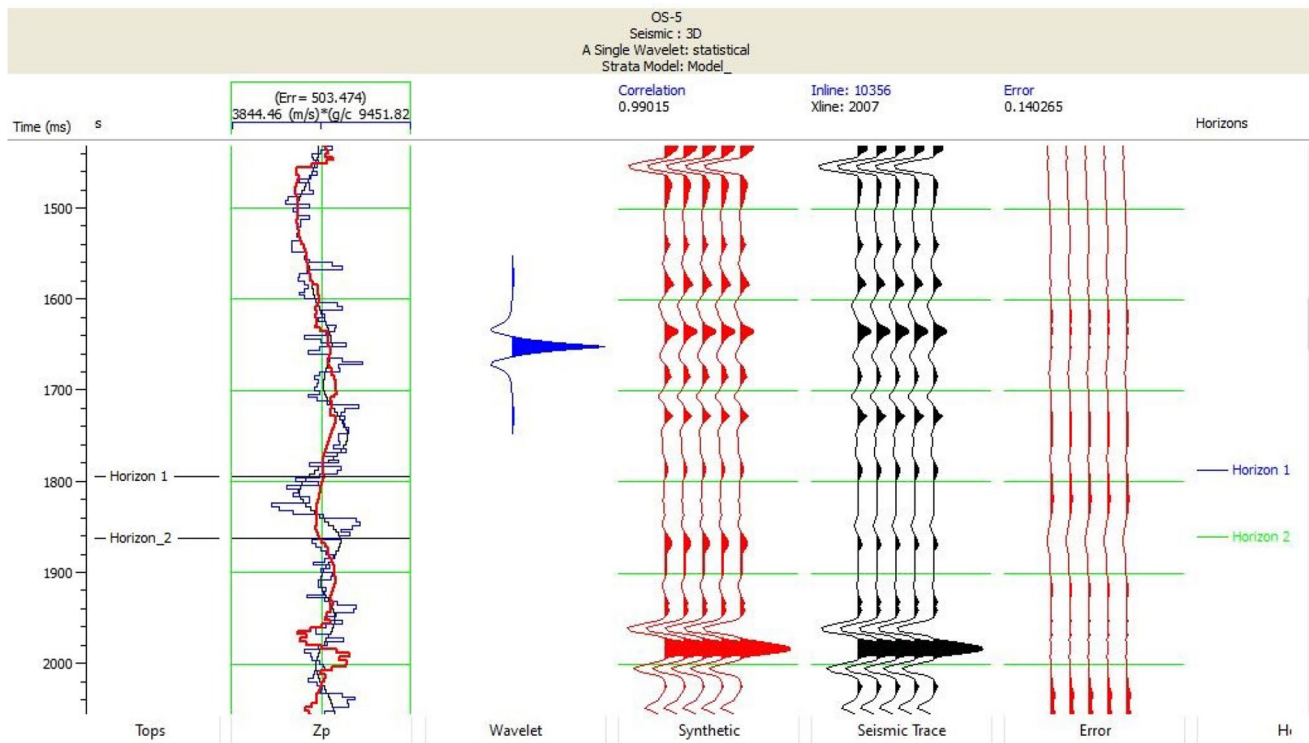
(c)

(d)

Fig. 11 (continued)

(e)

Fig. 11 (continued)

bodies. Additionally, fluid content plays a role, as hydrocarbon-filled sands exhibit lower impedance compared to water-bearing sands.

The inverted acoustic impedance attribute enables subsurface characterization by visualizing property variations across each horizon time slice, corresponding to potential reservoir tops in the 'OS' field (Fig. 15a–c). These horizon slices reveal that existing wells are situated in areas with low-to-moderate impedance values [3601–6727 (m/s)(g/cc)]. Well placement decisions were likely influenced by these impedance trends, with OS-1 and OS-5 deviated towards potential zones on horizon 1, OS-3 on horizon 2, and OS-2 and OS-5 on horizon 3. Based on typical characteristics of Niger Delta hydrocarbon reservoirs, areas with low impedance values below [6300 (m/s)(g/cc)] were identified as potential hydrocarbon-saturated sands. The horizon time slices (Fig. 15a–c) reveal several prospective zones with impedance values below this threshold. These zones hold the most significant hydrocarbon potential within the study area, with horizon 3 exhibiting the least prospective character. These newly identified prospective zones warrant further evaluation for potential drilling and development activities.

5 Conclusion

This study presented the application of seismic inversion and rock physics to characterize the subsurface reservoirs of an offshore field in the Niger Delta based on its hydrocarbon potential. Well log analysis identified three primary reservoir sands across five wells, exhibiting promising average reservoir properties, including gross thicknesses ranging from 49.2 to 81.4 m, net pay thicknesses from 26.4 to 73.8 m, and favourable porosity, permeability and water saturation values. Although Reservoir 1 showed the least favourable properties, the overall quality of the reservoirs indicates a strong hydrocarbon potential in the study area. The wavelet extraction through cross-correlation analysis identified a high-correlation statistical wavelet for seismic inversion, characterized by a 29° phase shift and a frequency range of 0–50 Hz. This wavelet was crucial for accurately estimating acoustic impedance from seismic data.

Quality control measures validated the robustness of the model-based seismic inversion process, demonstrating a strong correlation between well log impedance and seismic impedance, with a low error value range (385.225–520.235)
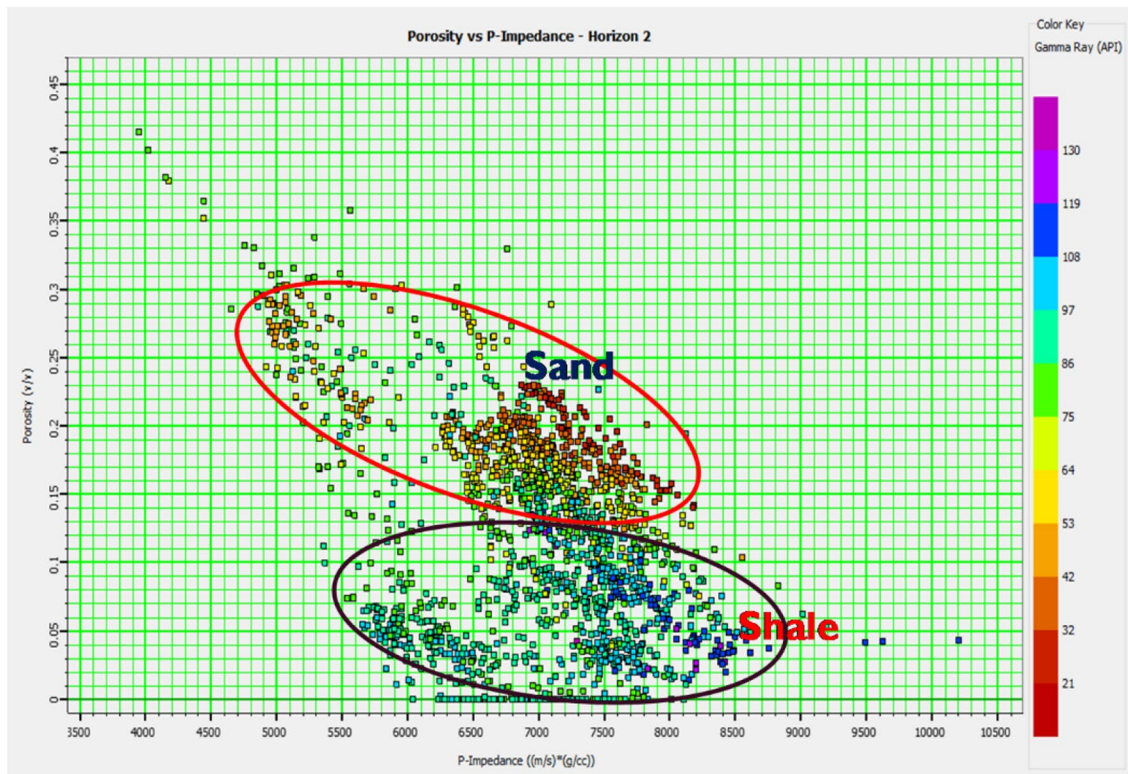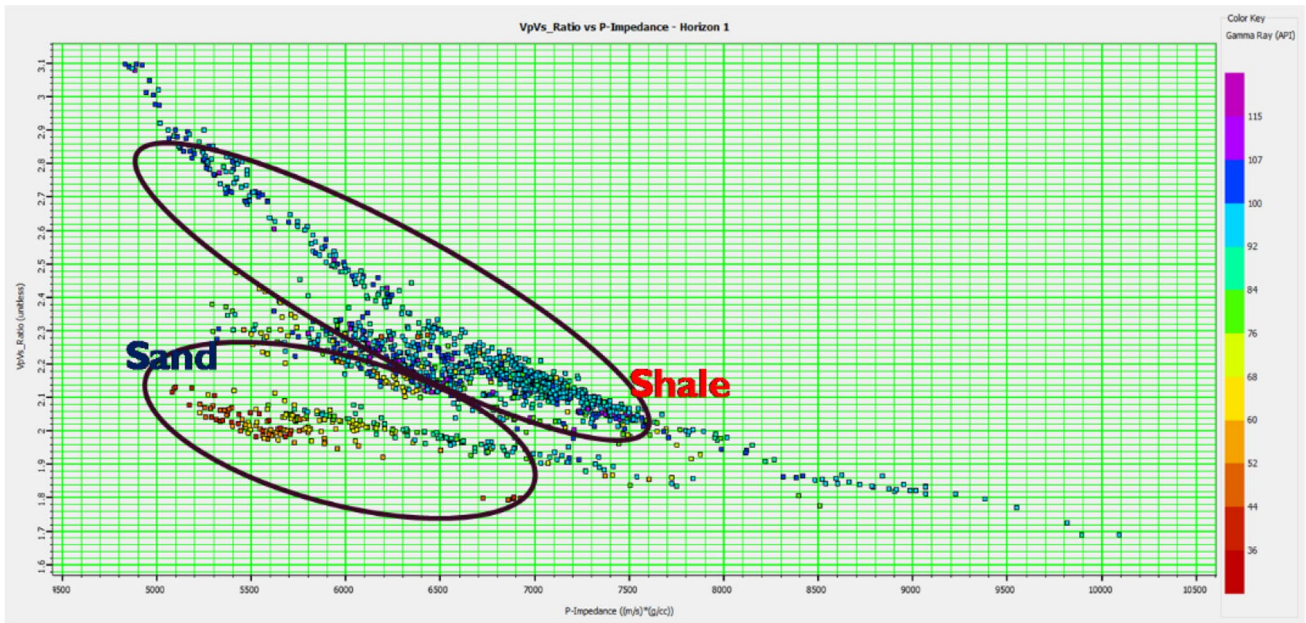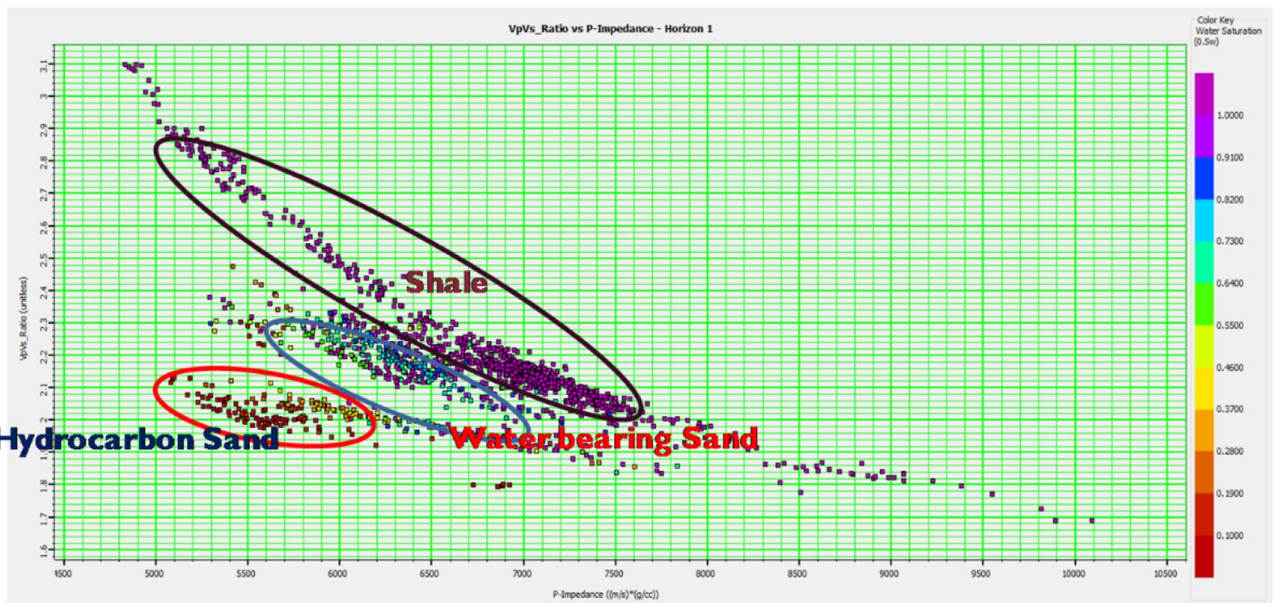
(a)
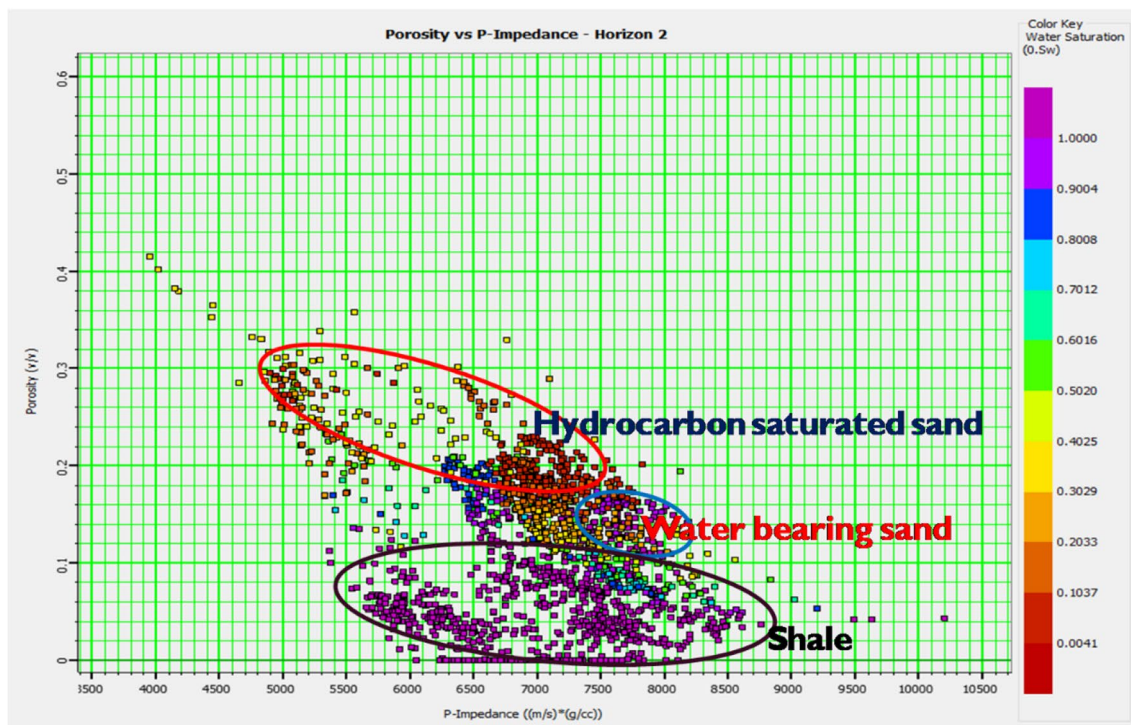
(b)

Fig. 12 A crossplot of porosity vs P-impedance coloured by **a** Gamma-ray values indicating the lithologies **b** water saturation values indicating the presence of fluid types

(a)

(b)

Fig. 13 A crossplot of the velocity ration (Vp/Vs) vs P-impedance (Zp) of horizon 1 coloured by **a** Gamma ray and **b** water saturation

and a high synthetic trace correlation range value of 0.983238 to 0.992808. Rock physics analysis in 3D space further clari-fied the relationships between rock properties, fluid content, and lithology. Cross-plots of P-impedance versus porosity and velocity ratio (Vp/Vs) facilitated the discrimination of lithologies and fluid contents, identifying hydrocarbon-bearing
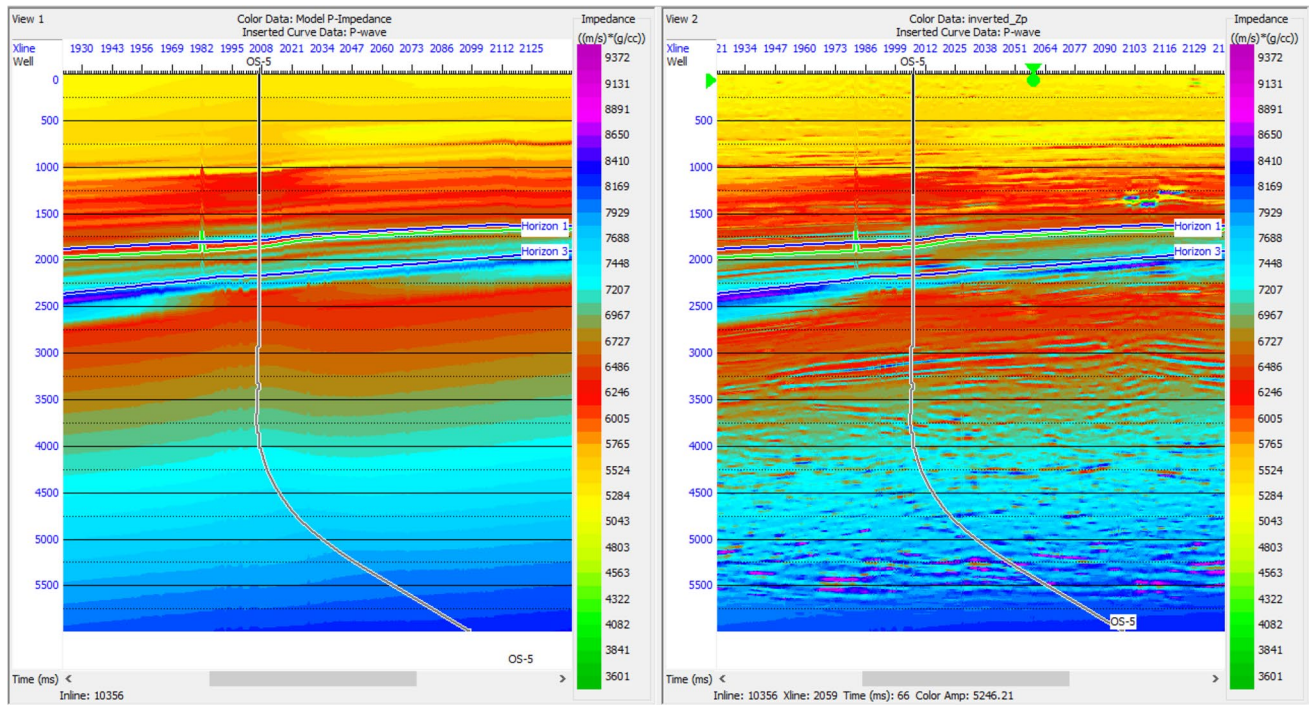
Fig. 14 **a** Initial low-frequency model used for the generation of inverted acoustic impedance volume of the 'OS' field and **b** inverted acoustic impedance seismic volume showing horizon 1 and horizon 3 and the position of OS-5
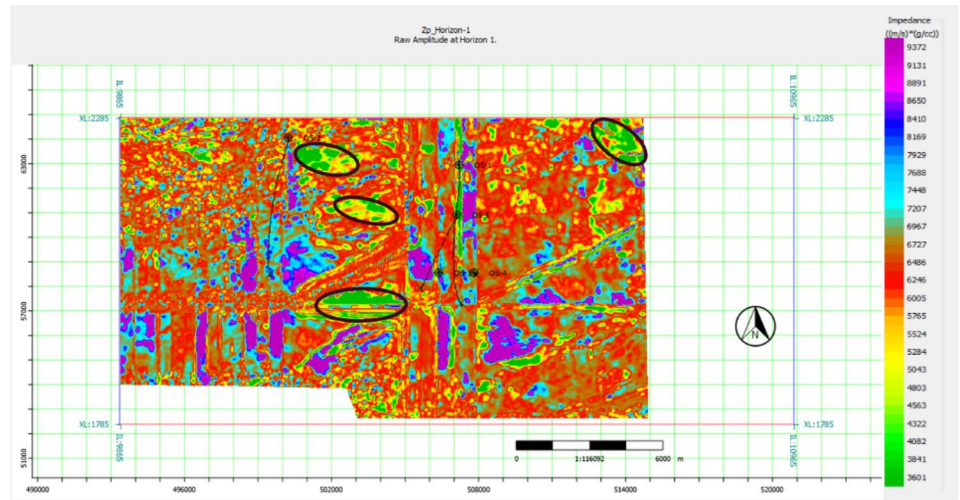
Table 2 Classification of acoustic impedance range for the inverted seismic

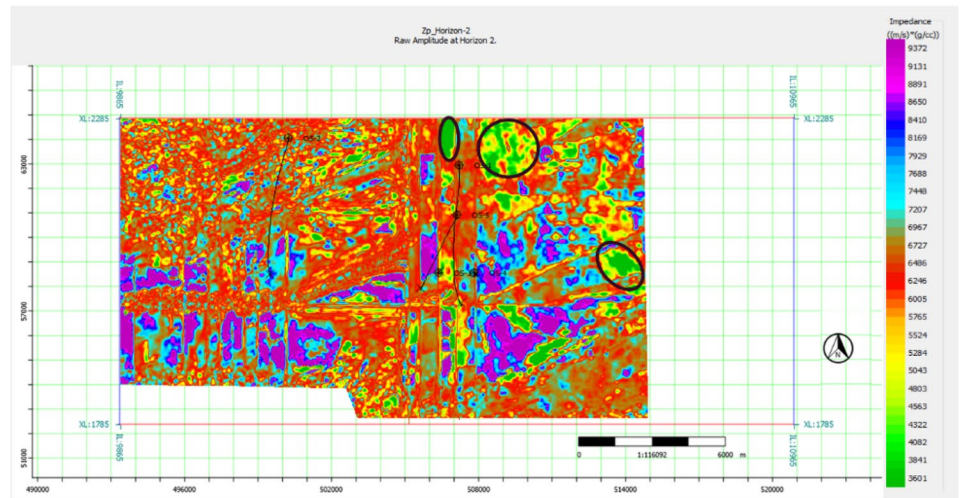| Acoustic impedance values (m/s)*(g/cc)	Category	Colour code
3601–4563	Very low	Green
4563–5765	Low	Yellow
5765–6967	Medium	Red
6967–7688	High	Aqua marine
7688–8650	Very high	Blue
8650–9372	Extremely high	Purple

sands, brine-saturated sands, and shales. Hydrocarbon sands were characterized by lower impedance values [5000–7000 (m/s)(g/cc)] compared to water-bearing sands [6800–8000 (m/s)(g/cc)] and shales [6000–9000 (m/s)(g/cc)].

The integration of these techniques yielded valuable insights into the subsurface. The inverted acoustic impedance sections displayed a clear increase in impedance with depth, reflecting the expected compaction trends. Furthermore, the impedance distribution across the mapped horizons revealed prospective zones with low impedance values [below 6300 (m/s)(g/cc)], particularly in horizons 1 and 2. This threshold was chosen because the rock physics analysis indicated significant overlaps in this range, effectively delineating hydrocarbon sands, brine-filled sands, and shale. The integrated approach of well log analysis, seismic inversion, and rock physics provides a robust framework for hydrocarbon exploration and development of prospective zones in the Niger Delta offshore field. The identified prospective zones offer promising targets for future exploration and drilling endeavours.
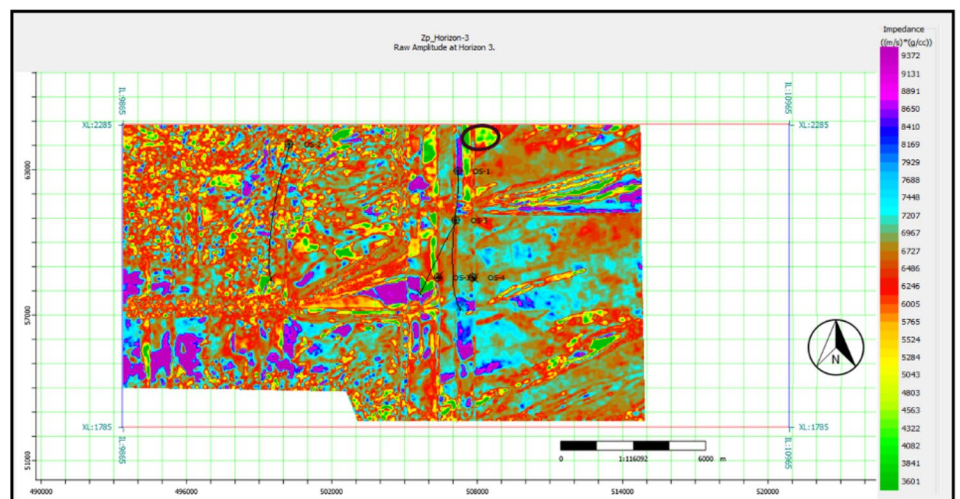
Fig. 15 Acoustic impedance horizon time slice showing hydrocarbon prospective zones encircled in black at OS-5 corresponding to the top of **a** reservoir 1 **b** reservoir 2 **c** reservoir 3

(a)

(b)

(c)

Data availability The data used for this study were obtained from a company (SPDC) through a national regulatory body (Nigerian Upstream Petroleum Regulatory Commission). The data for the field is proprietary and can be obtained from the company upon request. Due to privacy concerns, individual cannot release the data without their permission.

Declarations

Competing interests The authors declare that they have no competing interests.

References

1. El-Badri AS. The global energy outlook. Organisation of the Petroleum Exporting Countries (OPEC), October 28. IEA oil market reports: 1999, 2005. 2013. https://www.iea.org/media/omrreports/fullissues/.
2. Kantaatmadja BP, Nurhono AA, Majid RBA, Mohamad NYB, Amdan AB. Unlock hydrocarbon volumetric potential of LRLC clastic reservoirs in Malaysian Basins. In: Paper presented at the society of petroleum engineers—international petroleum technology conference 2014, IPTC 2014—innovation and collaboration: keys to affordable energy. 2014.
3. Ghaithan AM, Attia A, Duffuaa SO. Multi-objective optimization model for a downstream oil and gas supply chain. Appl Math Model. 2017;52:689–708.
4. Hussain M, Alamri A, Zhang T, Jamil I. Application of artificial intelligence in the oil and gas industry. In: Engineering applications of artificial intelligence. Springer Nature: Cham; 2024. p. 341–73.
5. Sinan S, Glover PW, Lorinczi P. Modelling the impact of anisotropy on hydrocarbon production in heterogeneous reservoirs. Transp Porous Media. 2020;133:413–36.
6. Sheykhinasab A, Mohseni AA, Barahooie Bahari A, Naruei E, Davoodi S, Aghaz A, Mehrad M. Prediction of permeability of highly heterogeneous hydrocarbon reservoir from conventional petrophysical logs using optimized data-driven algorithms. J Pet Explor Prod Technol. 2023;13(2):661–89.
7. Hammed O, Koledoye B, Ajao K, Ojero J, Jackson C, Sunday O, Adekunle A. Integrated 3D reservoir modeling for the delineation of sand body geometry and heterogeneity: implication for hydrocarbon potential assessment of "GMEDAL" field, offshore, Niger Delta. 2020.
8. Falade AO, Amigun JO, Makeen YM, Kafisanwo OO. Characterization and geostatistical modeling of reservoirs in 'Falad' field, Niger Delta, Nigeria. J Pet Explor Prod Technol. 2022;12(5):1353–69.
9. Akpan AS, Obiora DN, Okeke FN, Ibuot JC, George NJ. Influence of wavelet phase rotation on post stack inversion: a case study of X-field, Niger Delta, Nigeria. J Pet Gas Eng. 2020;11(1):57–67. https://doi.org/10.5897/JPGE2019.0320.
10. Hampson R. Hampson russell software theory. France: CGG Veritas Caractere; 2015.
11. Kiania I, Akpan AS. Delineation of hydrocarbon saturated reservoir sand using integrated 3d pre-stack seismic and well log data in Bonga-field, central Swamp Depobelt, Onshore Niger Delta, Nigeria. Malay J Geosci. 2020;5(2):64–8.
12. Ganguli SS, Dimri VP. Reservoir characterization: state-of-the-art, key challenges and ways forward. In: Developments in structural geology and tectonics, vol. 6. Amsterdam: Elsevier; 2024. p. 1–35.
13. Okeugo CG, Onuoha KM, Ekwe CA, Anyiam OA, Dim CIP. Application of crossplot and prestack seismic-based impedance inversion for discrimination of lithofacies and fluid prediction in an old producing field, Eastern Niger Delta Basin. J Pet Explor Prod Technol. 2019;9:97–110.
14. Ogbonna-Orji OC, Acra EJ, Adiela UP. Time-lapse evaluation of hydrocarbon production using rock properties and attributes in Niger Delta. Int J Sci Eng Sci. 2017;1:5–10.
15. Karim SU, Islam MS, Hossain MM, Islam MA. Seismic reservoir characterization using model-based post-stack seismic inversion: in case of Fenchuganj gas field, Bangladesh. J Japan Pet Inst. 2016;59(6):283–92.
16. Al-Ridha NA, Rasheed M. Porosity prediction from seismic inversion for Yamama Formation in (Abu-Amoud) oil field in southern of Iraq. Iraqi J Sci. 2018;59:1910–9.
17. Eze S, Orji OM, Nnorom SL, Ubogun K. Model based inversion of acoustic impedance from seismic trace for lithofacies differentiation: an application in Xy field offshore Niger Delta. J Appl Sci Environ Manag. 2019;23(9):1677–84.

18. Islam MS, Karim SU, Hossain MM. Seismic attributes analysis and evaluation of prospective hydrocarbon zones by seismic inversion in the Surma basin, Bangladesh. J Nat Sci Sustain Technol. 2018;12(4):249–61.

19. Shankar U, Ojha M, Ghosh R. Assessment of gas hydrate reservoir from inverted seismic impedance and porosity in the northern Hikurangi margin, New Zealand. Mar Petrol Geol. 2021;123: 104751.

20. Purnomo EW, Abdul Latiff AH, Elsaadany MMAA. Predicting reservoir petrophysical geobodies from seismic data using enhanced extended elastic impedance inversion. Appl Sci. 2023;13(8):4755.

21. Luo R, Chen H, Wang B. Semisupervised seismic impedance inversion with data augmentation and uncertainty analysis. Geophysics. 2023;88(4):M213–24.

22. Dai R, Yin C, Peng D. Elastic impedance simultaneous inversion for multiple partial angle stack seismic data with joint sparse constraint. Minerals. 2022;12(6):664.

23. Niu X, Zhang J, Liu J. Seismic impedance inversion in depth domain based on deep learning. Unconv Resour. 2023;3:72–83.

24. Zhang Y, Zhou H, Zhang M, Wang Y, Feng B, Liang M. Structurally constrained initial impedance modeling for poststack seismic inversion. IEEE Trans Geosci Remote Sens. 2023;61:1–10.

25. Ning J, Li S, Wei Z, Yang X. Multichannel seismic impedance inversion based on attention U-Net. Front Earth Sci. 2023;11:1104488.

26. Chi XG, Han DH. Lithology and fluid differentiation using a rock physics template. Lead Edge. 2009;28:60–5. https://doi.org/10.1190/1.3064147.

27. Abe SJ, Olowokere MT, Enikanselu PA. Development of model for predicting elastic parameters in 'bright' field, niger delta using rock physics analysis. NRIAG J Astron Geophys. 2018;7:264–78. https://doi.org/10.1016/j.nrjag.2018.05.006.

28. Akinyemi OD, Ayuk MA. Rock physics analysis as a tool for enhancing characterization of Niger Delta deep water sands. Arab J Geosci. 2022;15:98. https://doi.org/10.1007/s12517-021-09370-8.

29. Yu J, Duffaut K, Avseth P. Stress sensitivity of elastic moduli in high-porosity cemented sandstone—heuristic models and experimental data. Geophysics. 2023;88(4):MR185–94.

30. Wu C, Han L, Zhang F, Liu J, Chen H, Di B. Gas hydrate reservoir identification based on rock physics modelling and sensitive elastic parameters. J Geophys Eng. 2023;20(1):117–27.

31. Waqas M, Hou L, Ahmed JZ, Kumar S, Chatterjee S, Vargas N, et al. Rock physics modelling and stochastic seismic inversion to predict reservoir properties and quantify uncertainties of a complex upper Jurassic carbonate reservoir from offshore Abu Dhabi. In: SPE reservoir characterisation and simulation conference and exhibition?. SPE; 2023. p. D021S012R001.

32. Guo Z, Zhang T, Liu C, Liu X, Liu Y. Quantitative seismic interpretation of reservoir parameters and elastic anisotropy based on rock physics model and neural network framework in the shale oil reservoir of the Qianjiang Formation, Jianghan Basin, China. Energies. 2022;15(15):5615.

33. Tian L, Zhou D, Lin G, Jiang L. Reservoir prediction using poisson impedance in Qinhuangdao, Bohai Sea. In: SEG Denver 2010 annual meeting. 2010. p. 2261–4. https://doi.org/10.1190/1.3513300.

34. Oyeyemi KD, Olowokere MT, Aizebeokhai AP. Hydrocarbon resource evaluation using combined petrophysical analysis and seismically derived reservoir characterization, offshore Niger Delta. J Pet Explor Prod Technol. 2018;8:99–115. https://doi.org/10.1007/s13202-017-0391-6.

35. Nwachukwu J, Chukwura P. Organic matter of Agbada Formation, Niger Delta, Nigeria. AAPG Bull. 1986;70(1):48–55.

36. Evamy DDJ, Haremboure P, Kamerling WA, Knaap F, Molloy A, Rowlands MH. Hydrocarbon habitat of the tertiary Niger delta. AAPG Bull. 1978;62:1–39.

37. Short KC, Stauble A. Outline geology of Niger Delta. Am Assoc Pet Geol. 1967;51:761–76.

38. Stacher P. Present understanding of the Niger Delta hydrocarbon habitat. In: Oti MN, Postma G, editors. Geology of deltas. Rotterdam: A.A. Balkema; 1995. p. 257–67.

39. Xiao Y, Wang H. A new insight on sedimentary facies of the Miocene to Pliocene Agbada Formation, offshore Niger Delta Basin, Nigeria. J Afr Earth Sci. 2023;200: 104859.

40. Jika HT, Onuoha KM, Ibeneme SI, Adikwu SO, Okoro EM. Reservoir hydrocarbon potential of the Miocene Agbada Formation using RMS amplitude map and hydraulic flow unit model, Hatch field offshore, Niger Delta Basin, Nigeria. J Afr Earth Sci. 2022;196: 104682.

41. Avbovbo AA. Tertiary lithostratigraphy of Niger delta. AAPG Bull. 1978;62:295–306.

42. Shannon PM, Naylor N. Petroleum basin studies. London: Graham and Trotman Limited; 1989. p. 153–69.

43. Doust H, Omatsola E. Niger Delta. In: Edwards PA, Santogrossi PA, editors. Divergent and passive margin basins, vol. 45. America Association of Petroleum Geologists: Tulsa; 1990. p. 239–48.

44. Larionov VV. Borehole radiometry, vol. 127. Moscow: Nedra; 1969. p. 813.

45. Asquith GB, Krygowski D, Gibson CR. Basic well log analysis, vol. 16. Tulsa: American Association of Petroleum Geologists; 2004. p. 305–71.

46. Timur A. An investigation of permeability, porosity, and residual water saturation relationships. In: SPWLA annual logging symposium. SPWLA. 1968. p. SPWLA-1968.

47. Cooke D, Cant J. Model-based seismic inversion: comparing deterministic and probabilistic approaches. CSEG Rec. 2010;35(4):29–39.

48. Barclay F, Bruun A, Rasmussen KB, Alfaro JC, Cooke A, Cooke D, Salter D, Godfrey R, Lowden D, McHugo S, Ozdemir H, Pickering S, Pineda FG, Herwanger J, Volterrani S, Murineddu A, Rasmussen A. Seismic inversion reading between lines, spring. J-GLOBAL. 2008;20(1):42–63.

49. Goodway W, Chen T, Downton J. Improved AVO fluid detection and lithology discrimination using Lamé petrophysical parameters; λρ, μρ & λ/μ fluid stack from P and S inversions. In: 67th annual international meeting, SEG, expanded abstracts. 1997. p. 183–6. https://doi.org/10.1190/1.1885795.

50. Greenberg ML, Castagna JP. Shear wave velocity estimation in porous rocks: theoretical formulation, preliminary verification and applications. Geophys Prospect. 1992;40:195–209.

51. Mallick S. Model-based inversion of amplitude-variations-with-offset data using a genetic algorithm. Geophysics. 1995;60(4):939–54. https://doi.org/10.1190/1.1443860.

52. Jain C. Effect of seismic wavelet phase on post stack inversion. In: 10th biennial international conference & exposition, Kochi. 2013. p. 410

53. Illo CA, Onuoha MK. Rock-physics-model-based attributes and seismic inversion controls for reservoir characterization: a case study of 'Rhoda' field, Onshore Niger Delta Basin, Nigeria. Pet Coal. 2024;66(1):144–62.

54. Amjad MR, Zafar M, Malik MB, Naseer Z. Precise geopressure predictions in active foreland basins: an application of deep feedforward neural networks. J Asian Earth Sci. 2023;245: 105560.

55. Rai N, Singha DK, Chatterjee R. Assessment of Paleocene to lower Oligocene formations and basement to estimate the potential hydrocarbon reservoirs using seismic inversion: a case study in the Upper Assam Shelf, India. J Pet Explor Prod Technol. 2021;12:1–17.

56. Dagogo T, Ehirim CN, Ebeniro JO. Enhanced prospect definition using well and 4d seismic data in a Niger Delta field. Int J Geosci. 2016;7:977–90. https://doi.org/10.4236/ijg.2016.78074.

57. Oladele S, Salami R, Adeyemi OB. Petrophysical and rock physics analyses for characterization of complex sands in deep water Niger Delta. GeoSci Eng. 2019;65(2):24–35.